

CHARACTERISTICS OF ELASTIC WAVE PROPAGATION IN THICK BEAMS – WHEN GUIDED WAVES PREVAIL?

HAIKUO PENG

*Shanghai Jiao Tong University, State Key Laboratory of Mechanical System and Vibration,
Shanghai; and Shanghai Institute of Satellite Engineering, Shanghai, China
e-mail: penghaikuo@gmail.com*

LIN YE

*University of Sydney, Laboratory of Smart Materials and Structure (LSMS), School of Aerospace,
Mechanical and Mechatronic Engineering, Australia*

GUANG MENG, KAI SUN, FUCAI LI

*Shanghai Jiao Tong University, State Key Laboratory of Mechanical System and Vibration,
Shanghai, China*

Characteristics of wave propagation in thick beams are analyzed using a three-dimensional (3-D) spectral element method (SEM) for the purpose of damage detection. Analysis of wave propagation in beams of different thickness under excitations with different central frequency reveals that when the thickness of the beam is comparable to the wavelength of the elastic wave, a local wave mode, besides quasi-symmetric and quasi-anti-symmetric modes, exist simultaneously in the beam. In particular, when the wavelength is more than two times the beam thickness, the local wave modes are suppressed and the wave modes in the beam can be regarded as traditional guided waves, i.e., Lamb waves. It is demonstrated that the central frequency of wave signals can be selected according to the dimensions of the beam to obtain simple wave modes like those in thin beams. The characteristics of wave propagation in an intact beam and beams with a lateral crack are analyzed and the results are also validated by experiments, where wave propagation signals in thick steel beams are activated and captured using PZT elements.

Key words: wave propagation, spectral element method, thick beam, damage detection

1. Introduction

For structures in aerospace, civil and infrastructure applications, abrupt impact or growth of fatigue defects during service life can result in catastrophic failure. It is therefore essential to develop techniques of surveilling the integrity

of these structures and improving their safety and reliability. Various structural health monitoring (SHM) methods have been developed (Inman *et al.*, 2005; Staszewski *et al.*, 2009; Su and Ye, 2009). Due to the long-range propagation potential of elastic waves and their sensitivity to a variety of damage, elastic-wave-based techniques for damage detection received a considerable attention in the past decades (Giurgiutiu, 2003; Kessler *et al.*, 2002; Raghavan and Cesnik, 2007; Su *et al.*, 2006).

For elastic-wave-based damage detection techniques, it is essential to understand the wave propagation characteristics in structures to be examined. A number of numerical methods have been applied to analyze the propagation of elastic waves in various types of structures (Lee and Staszewski, 2003a,b). The orthogonal polynomials (e.g., Legendre and Chebyshev polynomials) -based SEM, proposed by Patera (1984), which take advantage of the accuracy of the spectral method and conserves the flexibility of FEM, are much more suitable for analyzing wave propagation in a medium with complex geometry than the conventional FEM. This method has been successfully applied in many areas, such as fluids (Canuto *et al.*, 1988; Fischer *et al.*, 2002; Karniadakis and Sherwin, 2005), seismology (Komatitsch *et al.*, 2002; Komatitsch and Vilotte, 1998; Seriani, 1998) and acoustics (Seriani and Priolo, 1994). In the past few years, the SEM was used to simulate wave propagation in structures for the purpose of damage detection. For example, wave propagation in 1-D structures such as rods (Sridar *et al.*, 2006) and beams (Kudela *et al.*, 2007b), 2-D structures such as isotropic (Zak *et al.*, 2006) and composite plate (Kudela *et al.*, 2007a) was investigated using SEM. Wave propagation in 2-D plate structures using three-dimensional SEM for damage detection was also discussed in Peng *et al.* (2009). PZT transducers were modeled using SEM to generate and receive Lamb waves (Ha and Chang, 2010b; Kim *et al.*, 2008; Kudela and Ostachowicz, 2009) and the effect of the adhesive layer between a PZT and a host structure was discussed (Ha and Chang, 2010a).

Thick beams play important roles in 3-D structures. Unlike the beam structures that are commonly considered, where the wavelength of the elastic waves is much greater than the thickness of the beam, the cross-section size of thick beams is comparable to the wavelength. In this paper, thick beams are modeled using the Legendre-polynomials-based 3-D SEM and elastic wave propagation characteristics are analyzed. The characteristics of elastic wave propagation in beams with and without a crack are evaluated. Subsequently, the simulation results are validated with experimental results.

2. Formulation of the spectral element method

As in the conventional FE method, SEM first requires the domain Ω in three dimensions to be decomposed into a number of non-overlapping elements Ω_e . Each element in the physical domain is mapped to a reference domain $\Lambda = [-1, 1]^3$ with local coordinates using an invertible local mapping function f . One difference between the SEM and FEM is the distribution of nodes. A set of nodes is defined as $\xi_i \in [-1, 1], i = 1, \dots, N + 1$ in the domain Λ . In SEM, these Gauss-Lobatto-Legendre (GLL) points are the $(N + 1)$ roots of (Canuto *et al.*, 1988)

$$(1 - \xi^2)P'_N(\xi) = 0 \tag{2.1}$$

where $P'_N(\xi)$ is the derivative of the Legendre polynomial of the degree N . Those nodes are irregularly distributed, while the nodes are uniformly spaced in FEM.

In a 3-D spectral finite element, the basis function can be written as

$$\psi_{ijk} = h_i(\xi_p)h_j(\eta_q)h_k(\gamma_r) = \begin{cases} 1 & i = p, \quad j = q, \quad k = r \\ 0 & \text{otherwise} \end{cases} \tag{2.2}$$

$h_m(\xi)$ denotes the m -th 1-D Lagrange interpolation at the $(N+1)$ GLL points. As an example, a 125-node spectral element in the local coordinate system is shown in Fig. 1.

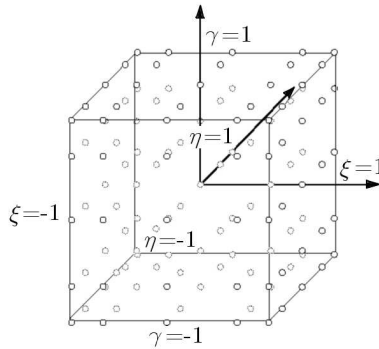


Fig. 1. A 125-node spectral finite element in the local coordinate system

Therefore, the integrals for the element matrices, \mathbf{M}^e , \mathbf{K}^e and \mathbf{F}^e , are calculated numerically in the local coordinate

$$\begin{aligned}
\mathbf{M}^e &= \rho \sum_{i=1}^{n_1} \omega_i \sum_{j=1}^{n_2} \omega_j \sum_{k=1}^{n_3} \omega_k [\boldsymbol{\Psi}^e(\xi_i, \eta_j, \gamma_k)]^\top [\boldsymbol{\Psi}^e(\xi_i, \eta_j, \gamma_k)] \det \mathbf{J}_e^{ijk} \\
\mathbf{K}^e &= \sum_{i=1}^{n_1} \omega_i \sum_{j=1}^{n_2} \omega_j \sum_{k=1}^{n_3} \omega_k [\mathbf{B}^e(\xi_i, \eta_j, \gamma_k)]^\top \mathbf{C} [\mathbf{B}^e(\xi_i, \eta_j, \gamma_k)] \det \mathbf{J}_e^{ijk} \quad (2.3) \\
\mathbf{F}^e &= \sum_{i=1}^{n_1} \omega_i \sum_{j=1}^{n_2} \omega_j \sum_{k=1}^{n_3} \omega_k [\boldsymbol{\Psi}^e(\xi_i, \eta_j, \gamma_k)]^\top \mathbf{P}(\xi_i, \eta_j, \gamma_k) \det \mathbf{J}_e^{ijk}
\end{aligned}$$

where ρ is the mass density, \mathbf{C} is the material stiffness matrix, and \mathbf{P} is the distributed load. $\boldsymbol{\Psi}^e$ are the shape functions based on the Legendre polynomials. The matrix \mathbf{B}^e is the strain-displacement matrix. \mathbf{J}_e is the Jacobian matrix associated with the mapping function f from the physical domain Ω_e to the reference domain Λ . ω_i is the weights of the GLL quadrature (Komatitsch *et al.*, 2000; Pozrikidis, 2005). n_i , $i = 1, 2, 3$ are the numbers of GLL points in each direction in the local coordinate.

If we let \mathbf{U}^e denote the elementary vector of an unknown displacement in the medium for wave propagation, the ordinary dynamic equation can be written as (Pozrikidis, 2005)

$$\mathbf{M}^e \ddot{\mathbf{U}}^e + \mathbf{K}^e \mathbf{U}^e = \mathbf{F}^e \quad (2.4)$$

where \mathbf{M}^e denotes the elementary mass matrix, \mathbf{K}^e is the elementary stiffness matrix, and \mathbf{F}^e is the vector of time-dependent excitation force.

In a structural health monitoring system, the PZT transducer can be used as an actuator as well as a sensor. The converse piezoelectric effect of piezoelectric materials, which converts an externally applied electric field into induced strain, and the direct piezoelectric effect, which generates an electric field under deformation, can be adopted for actuator and sensor correspondingly. According to constitutive equations for piezoelectric materials, the elementary governing equations of motion (2.4) can be rewritten as follows (Kudela and Ostachowicz, 2009; Wang, 2004)

$$\begin{aligned}
\mathbf{M}^e \ddot{\mathbf{U}}^e + \mathbf{K}^e \mathbf{U}^e - \mathbf{K}_{u\phi}^e \phi^e &= \mathbf{F}^e \\
\mathbf{K}_{\phi u}^e \mathbf{U}^e + \mathbf{K}_{\phi}^e \phi^e &= \mathbf{Q}^e
\end{aligned} \quad (2.5)$$

The piezoelectric coupling matrices $\mathbf{K}_{u\phi}^e$ and $\mathbf{K}_{\phi u}^e$ and dielectric permittivity matrix \mathbf{K}_{ϕ}^e can be calculated as

$$\begin{aligned}
 \mathbf{K}_{u\phi}^e &= (\mathbf{K}_{\phi u}^e)^\top = - \int_{\Omega_e} \mathbf{B}^\top \mathbf{e}^\top \mathbf{B}_\phi d\Omega_e = \\
 &= - \sum_{i=1}^{n_1} \omega_i \sum_{j=1}^{n_2} \omega_j \sum_{k=1}^{n_3} \omega_k [\mathbf{B}(\xi_i, \eta_j, \gamma_k)]^\top \mathbf{e}[\mathbf{B}_\phi(\xi_i, \eta_j, \gamma_k)] \det \mathbf{J}_e^{ijk} \\
 \mathbf{K}_\phi^e &= \int_{\Omega_e} \mathbf{B}_\phi^\top \mathbf{g} \mathbf{B}_\phi d\Omega_e = \\
 &= \sum_{i=1}^{n_1} \omega_i \sum_{j=1}^{n_2} \omega_j \sum_{k=1}^{n_3} \omega_k [\mathbf{B}_\phi(\xi_i, \eta_j, \gamma_k)]^\top \mathbf{g}[\mathbf{B}_\phi(\xi_i, \eta_j, \gamma_k)] \det \mathbf{J}_e^{ijk}
 \end{aligned}
 \tag{2.6}$$

where \mathbf{e} is the piezoelectric constant matrix; \mathbf{g} the dielectric constant matrix, \mathbf{Q}^e the nodal externally applied charge vector.

According to the displacement and traction boundary on the surface of both the host structure and piezoelectric transducer as well as electric potential and charge boundary on the surface of the piezoelectric transducer, the elementary governing equations of motion can be solved using a central difference time integration scheme (Peng *et al.*, 2009).

3. Wave propagation analysis in a thick beam

The wave propagation characteristics in steel beams of 34 mm (thickness) \times 25 mm (width) \times 300 mm (length), shown in Fig. 2, are investigated. The steel density ρ is 7900 kg/m³, Young’s modulus E is 200 GPa, and Poisson ratio ν is 0.3. The beam is modeled using 4 (thickness) \times 5 (width) \times 30 (length) elements with $5 \times 5 \times 5$ nodes, as depicted in Fig. 1. In this model, damping is not considered and the boundaries are free.



Fig. 2. Geometric configuration of the steel beam [mm]

3.1. Elastic wave propagation in an intact thick beam

First, an intact beam is excited by a single shear force applied at the point A on the upper surface at the left-hand end of the beam, as shown in Fig. 2. A

Hanning-windowed 3.5-cycle sinusoidal toneburst with the central frequency of 35 kHz is used as the excitation signal. The waveform of the excitation signal in the time domain is shown in Fig. 3. The displacement components of response in the beam in the x direction at the times of 0.050 ms, 0.079 ms, 0.106 ms and 0.141 ms are shown in Fig. 4. It can be seen that the elastic waves propagating in the beam experience repeated reflections at the upper and lower surfaces alternately, and then they are reflected by the right-hand end of the beam. Wave propagation in the mid-plane in the width direction is illustrated in Fig. 5. When the beam is excited, the main longitudinal wave and main shear wave with reflections between the upper and lower surfaces can be observed. Superposition of their reflections and the possible converted longitudinal waves and shear waves constitute the formulation of quasi-symmetrical (quasi-S) wave mode associated with the longitudinal mode and quasi-anti-symmetrical (quasi-A) wave mode associated with the flexible mode in the thick beam.

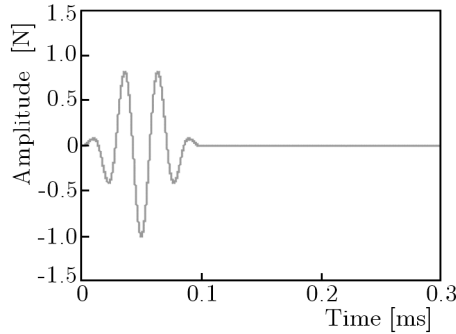


Fig. 3. Waveform of the excitation signal in the time domain

Two points, named B and B' , which are symmetric with respect to the mid-plane in the thickness direction, as shown in Fig. 2, are selected to investigate wave propagation in the beam. The displacement components in the x direction at the points B and B' are shown in Fig. 6. The incident wave and the reflected wave from the right-hand end of the beam can be observed in the responses of B and B' . As in the thin beam, both symmetrical and anti-symmetrical modes can be excited simultaneously by the single shear force of the input signal. However, the amplitudes of the displacement at both points are neither exactly identical nor opposite, which is the reason why these wave modes are called quasi-S mode and quasi-A mode in the present study. Under the excitation with a central frequency of 35 kHz, the group velocities of the quasi-S mode and quasi-A mode are about 5210 m/s and 3068 m/s, respectively, calculated using the arrival time (captured at point B) of the wave packets

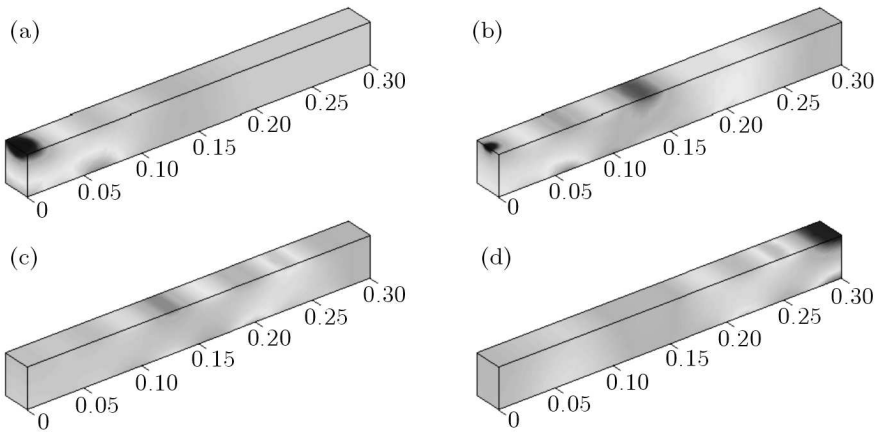


Fig. 4. Displacement component in the x direction of the intact beam at (a) 0.050 ms; (b) 0.079 ms; (c) 0.106 ms; (d) 0.141 ms

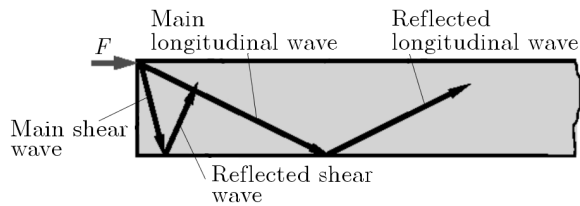


Fig. 5. Reflections of elastic waves in the thick beam

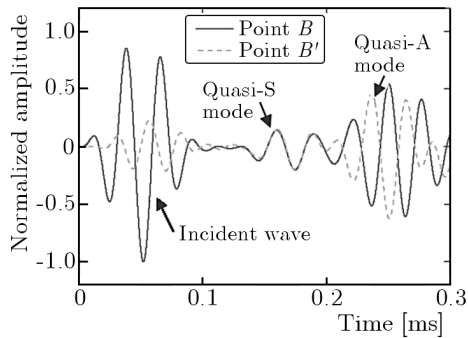


Fig. 6. Displacement components in the x direction of the intact beam at points B and B' under the excitation of a single shear force

reflected from the right-hand end of the beam. As expected, the quasi-S modes travel more quickly than the quasi-A modes. In addition, the quasi-A mode is dominant in wave propagation, with its normalized magnitude (0.543) being clearly greater than that of quasi-S mode (0.148).

3.2. Effects of the excitation frequency and thickness

In the beam with a large thickness, the characteristics of wave propagation become more complex when the excitation frequency is increased. For example, an excitation with a central frequency of 56 kHz is used. Under such an excitation, the local wave mode can be observed as shown in Fig. 7. The reason for the occurrence of the local wave mode is that the elastic waves reflect directly from the upper and lower surfaces. In this case, the reflected waves of the local wave mode overlap with the reflected wave from the right-hand end of the beam. The response at point *B* in Fig. 8 clearly shows the signals of the local wave mode immediately after the incident wave.

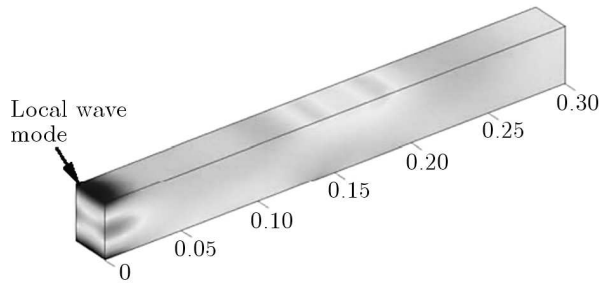


Fig. 7. Displacement component in the x direction of the intact beam at 0.078 ms under the excitation with a central frequency of 56 kHz

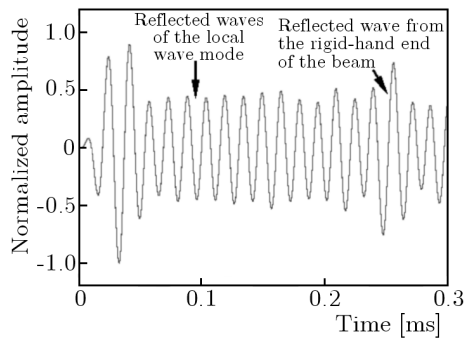


Fig. 8. Displacement component in the x direction at the point *B* under the excitation with a central frequency of 56 kHz

For the purpose of damage detection using an elastic wave, simple wave modes with a long range of propagation are desired. To obtain the simple modes of wave propagation in a thick beam, the excitation frequency should be carefully selected to avoid the local wave mode.

To evaluate the local wave mode in detail, three beams with thicknesses of 28 mm, 34 mm and 40 mm are activated using a shear force with frequencies from 25 kHz to 70 kHz with a step of 5 kHz. Three curves of the normalized magnitude of the local wave mode at the point B as a function of the excitation frequency are plotted in Fig. 9a. It is evident that the normalized magnitude of the local wave mode is small at low frequencies. With an increase in the excitation frequency, the magnitude increases significantly from a particular frequency for the beams of different thickness, indicating that the existence of the local wave mode is dependent on the excitation frequency f and the thickness of the beam h . When the normalized magnitudes of the local wave mode are plotted as a function of L_w/h , as shown in Fig. 9b, it is interesting to see that the three curves merge into one, where L_w is calculated as

$$L_w = \frac{c_L}{f} \tag{3.1}$$

where c_L is the wave speed of shear wave in the steel material and f is the excitation frequency. One essential observation here is that if the wavelength L_w , of the shear wave is about more than two times the thickness of the beam h , the normalized magnitude of the local wave mode becomes very small, indicating that the local wave mode are almost invisible, and in particular, a simple wave mode (i.e. Lamb waves) like those in thin beams can be obtained.

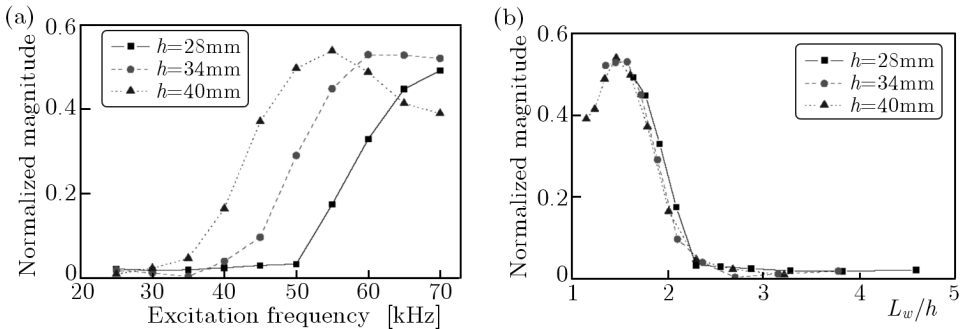


Fig. 9. Normalized magnitude of the local wave mode as functions of (a) excitation frequency f and (b) L_w/h

According to the above conclusion, to prevent the occurrence of local wave mode, for beams with a thickness of 28 mm, 34 mm and 40 mm, when

$L_w/h \geq 2$, the corresponding excitation frequencies should be less than about 57 kHz, 47 kHz and 40 kHz, respectively. It is worth mentioning that when the excitation frequency is greater than 64 kHz for beams with a width of 25 mm, the wavelength of the shear wave $L_w < 50$ mm, which is less than two times the width, and a local wave mode symmetric about the mid-plane in the width direction is also formulated because the elastic waves are also reflected by the two side surfaces of the beam, similar to the case in the thickness direction.

3.3. Wave propagation under the excitation of PZT actuator

In a structural health monitoring system, the PZT transducer is commonly used to generate and capture Lamb wave signals. In this study, two PZT transducers are modeled using the spectral element method. The dimensions of the PZT transducer (PIC151) are 20 mm (length) \times 5 mm (width) \times 1 mm (thickness). One PZT transducer acts as an actuator and another one act as a sensor, as show in Fig. 10. An excitation signal of Hanning-windowed 3.5-cycle sinusoidal toneburst with the magnitude of 30 V is applied to the upper surface of the PZT actuator. Displacement responses of the structure and PZT transducer in the x direction at 0.058 ms are shown in Fig. 11. A large displacement can be observed in two ends of the PZT actuator.

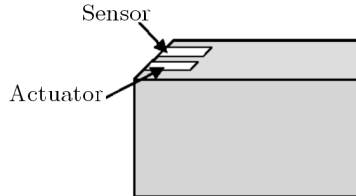


Fig. 10. Schematic diagram of the coupled PZT-structure excitation model

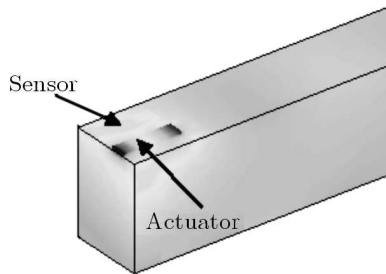


Fig. 11. Displacement response of the structure and PZT transducer in the x direction at 0.058 ms

Figure 12 shows the output voltage signal of sensor in the intact beam under the excitation of PZT actuator. Similar to the case under excitation of single shear force, there are three wave packets in the captured signal. The first one is the incident wave; the second one is the quasi-S mode and the third one is the quasi-A mode. The magnitude of the quasi-A mode is obviously larger than the quasi-S mode.

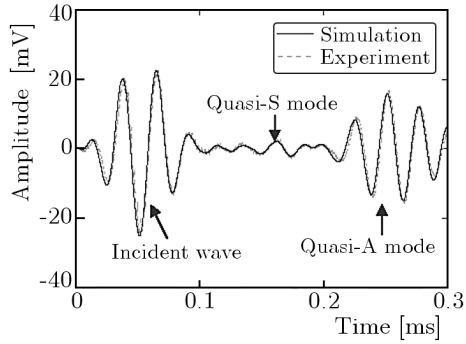


Fig. 12. Captured signal of the sensor in the intact beam under excitation of the PZT actuator with the central frequency of 35 kHz

As described before, when the excitation frequency is increased, a local wave mode will appear under the excitation of a point shear force. Under the excitation of the PZT actuator, when the central frequency of excitation is increased to 56 kHz, the local wave mode can also be observed, as shown in Fig. 13. The signal is very complex because of the local wave mode.

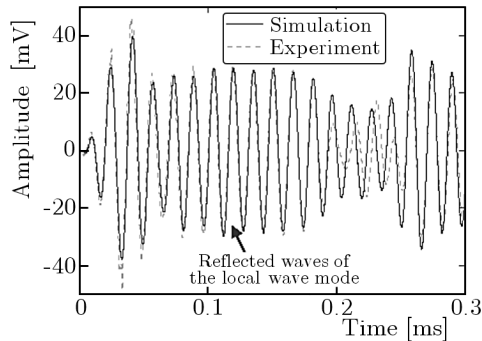


Fig. 13. Captured signal of the sensor in the intact beam under excitation of the PZT actuator with the central frequency of 56 kHz

4. Elastic wave propagation in beams with a lateral crack

Wave propagation in beams with a lateral crack located in the middle of the beam, shown in Fig. 14, are investigated next. The degree of the damage is defined by d/h , where d is the depth of the crack and h is the thickness of the beam. Here, $h = 34$ mm. Two cases with degrees of damage of 25% and 50% are considered. The crack in the beam is modeled by the nodes separation method, schematically shown in Fig. 15. Initially, the structure is meshed without the crack. The nodes exactly on the crack plane are duplicated and attached to the adjacent elements.

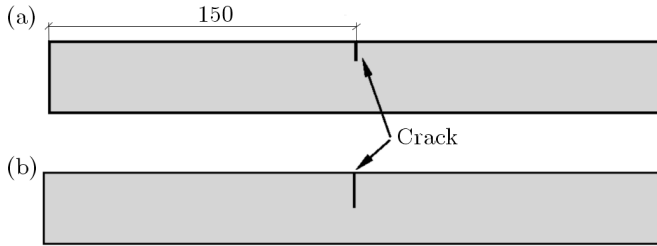


Fig. 14. Crack in the beam with degree of damage: (a) 25%; (b) 50% [mm]

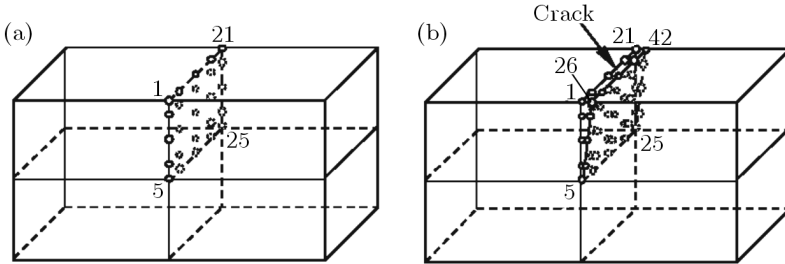


Fig. 15. Modeling of the crack: (a) mesh without crack; (b) mesh with crack

Under the excitation with a central frequency of 35 kHz, the captured signals of the sensor are presented in Figs. 16 and 17. The reflected signal from damage can be observed between the incident wave packet and the reflected wave packet from the right-hand end of the beam. It is mainly the reflection of the quasi-A mode for that the quasi-A mode dominates the wave propagation under the excitation with the central frequency of 35 kHz, as discussed previously. The normalized magnitude (0.25) of the wave reflected from the crack in the case of a 50% degree of damage is greater than that (0.20) for the 25% degree of damage. It is worth mentioning that the reflected wave of the

quasi-S mode with a small magnitude from the right-hand end of the beam and the reflected wave of the quasi-A mode from the crack overlap each other.

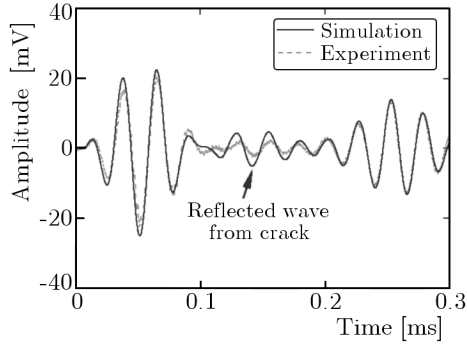


Fig. 16. Captured signal of the sensor in the beam with 25% damage degree under the excitation with a central frequency of 35 kHz

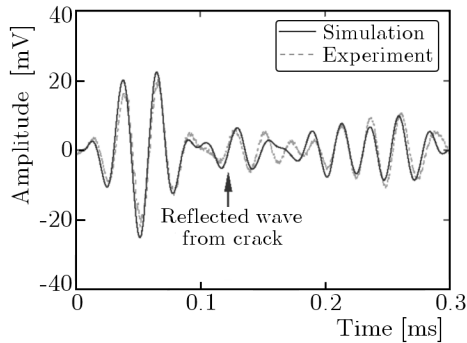


Fig. 17. Captured signal of the sensor in the beam with 50% damage degree under the excitation with a central frequency of 35 kHz

5. Experimental validation

Three steel beams with dimensions shown in Fig. 2 are used to validate the wave propagation characteristics in thick beams. One specimen is kept intact as a benchmark, and the other two are cut in the mid-span with a notch to simulate the crack. The depths of the notches are 8mm and 17mm, to simulate cracks of 25% and 50% degrees of damage, respectively. Two pieces of the PZT (PI®PIC151, PQYY-0586) element are surface-mounted on the upper surface

at the left-hand end of each specimen. One serves as the actuator to generate elastic waves while the other serves as the sensor to acquire the reflected wave signals in the steel beams. The generation and acquisition of elastic wave signals are fulfilled using an active signal generation and data acquisition system developed on the VXI platform, consisting mainly of a signal generation unit (Agilent©E1441), signal amplifier (PiezoSys®EPA-104), signal conditioner (Agilent©E3242A) and signal digitizer (Agilent©E1437A). 3.5-cycle sinusoidal tonebursts enclosed in a Hanning window with a magnitude of 30V as used in simulation are generated and applied to the PZT actuator.

Under the excitation with a central frequency of 35 kHz, the captured signal in the experiments for intact beam is shown in Fig. 12. The simulation results are in good agreement with the experimental results, in which both quasi-S mode and quasi-A mode can be observed. When the central frequency is increased to 56 kHz, the captured signal is more complex, as shown in Fig. 13, and it has a similar profile as the simulation signal, indicating the existence of the local wave mode. When there is a notch in the beam, the elastic wave is reflected from both the damage and the right-hand end of the beam, shown in Figs. 16 and 17. When the degree of damage is 50%, the normalized magnitude of the reflection from the damage (0.31) is greater than that of the beam with degree of damage of 25% (0.15), as predicted by the simulation results, indicating that the magnitude of the reflected wave from crack can convey information about the degree of damage in such a 3-D structure. Therefore, the effectiveness of the proposed SEM model is validated by the good agreement in general trends between the simulation and experiment results.

6. Conclusions

Characteristics of wave propagation in thick beams are analyzed. It is shown that the characteristics of wave propagation in thick beams are complex, with the interaction between local wave modes, quasi-symmetric and quasi-anti-symmetric wave modes, when the thickness of the beam is comparable to the wavelength of the elastic wave. In particular, when the shear wavelength is two times the beam thickness, the local wave modes are suppressed and the wave modes in the beam can be regarded as traditional guided wave modes, i.e. Lamb waves. Therefore, the excitation frequency should be carefully selected when carrying out damage detection strategies for such thick beams. A lateral crack in thick beams is modeled using a node separation method, and the interaction of elastic wave with the lateral crack is analyzed. The simulation

results of wave propagation in thick beams are validated by experiments, where the wave propagation in a thick steel beam is activated and captured using PZT elements.

Acknowledgements

The authors are grateful for the support received from the National Natural Science Foundation of China (NSFC No. 11072148, 11061160491), the National High Technology Research and Development Program of China (863 Program, No. 2009AA044800) and Research Project of State Key Laboratory of Mechanical System and Vibration (MSV201110).

References

1. CANUTO C., QUARTERONI A., HUSSAINI M.Y., ZANG T.A., 1988, *Spectral Methods in Fluid Dynamics*, Berlin: Springer
2. FISCHER P., KRUSE G., LOTH F., 2002, Spectral element methods for transitional flows in complex geometries, *Journal of Scientific Computing*, **17**, 1, 81-98
3. GIURGIUTIU V., 2003, Lamb wave generation with piezoelectric wafer active sensors for structural health monitoring, *Smart Structures and Materials: Smart Structures and Integrated Systems*, **5056**, 111-122
4. HA S., CHANG F., 2010a, Adhesive interface layer effects in PZT-induced Lamb wave propagation, *Smart Materials and Structures*, **19**, p. 025006
5. HA S., CHANG F., 2010b, Optimizing a spectral element for modeling PZT-induced Lamb wave propagation in thin plates, *Smart Materials and Structures*, **19**, p. 015015
6. INMAN D.J., FARRAR C.R., LOPES J.V., STEFFEN J.V., 2005, *Damage Prognosis: for Aerospace, Civil and Mechanical Systems*, John Wiley & Sons, Ltd.
7. KARNIADAKIS G., SHERWIN S., 2005, *Spectral/hp Element Methods for Computational Fluid Dynamics*, Oxford University Press, USA
8. KESSLER S.S., SPEARING S.M., SOUTIS C., 2002, Damage detection in composite materials using Lamb wave methods, *Smart Materials and Structures*, **11**, 2, 269-278
9. KIM Y., HA S., CHANG F., 2008, Time-domain spectral element method for built-in piezoelectric-actuator-induced Lamb wave propagation analysis, *AIAA Journal*, **46**, 3, 591-600

10. KOMATITSCH D., BARNES C., TROMP J., 2000, Simulation of anisotropic wave propagation based upon a spectral element method, *Geophysics*, **65**, 4, 1251-1260
11. KOMATITSCH D., RITSEMA J., TROMP J., 2002, The spectral-element method, Beowulf computing, and global seismology, *Science*, **298**, 5599, 1737-1742
12. KOMATITSCH D., VILOTTE J., 1998, The spectral element method: an efficient tool to simulate the seismic response of 2D and 3D geological structures, *Bulletin of the Seismological Society of America*, **88**, 2, 368-392
13. KUDELA P., KRAWCZUK M., OSTACHOWICZ W., 2007b, Wave propagation modelling in 1D structures using spectral finite elements, *Journal of Sound and Vibration*, **300**, 88-100
14. KUDELA P., OSTACHOWICZ W., 2009, *3D Time-Domain Spectral Elements for Stress Waves Modelling*, Institute of Physics Publishing
15. KUDELA P., ZAK A., KRAWCZUK M., OSTACHOWICZ W., 2007a, Modelling of wave propagation in composite plates using the time domain spectral element method, *Journal of Sound and Vibration*, **302**, 728-745
16. LEE B.C., STASZEWSKI W.J., 2003a, Modelling of Lamb waves for damage detection in metallic structures: Part I. Wave propagation, *Smart Materials and Structures*, **12**, 5, 804-814
17. LEE B.C., STASZEWSKI W.J., 2003b, Modelling of Lamb waves for damage detection in metallic structures: Part II. Wave interactions with damage, *Smart Materials and Structures*, **12**, 5, 815-824
18. PATERA A.T., 1984, A spectral element method for fluid dynamics: laminar flow in a channel expansion, *Journal of Computational Physics*, **54**, 468-488
19. PENG H.K., MENG G., LI F.C., 2009, Modeling of wave propagation in plate structures using three-dimensional spectral element method for damage detection, *Journal of Sound and Vibration*, **320**, 4/5, 942-954
20. POZRIKIDIS C., 2005, *Introduction to Finite and Spectral Element Methods Using MATLAB*, CRC Press
21. RAGHAVAN A., CESNIK C., 2007, Review of guided-wave structural health monitoring, *The Shock and Vibration Digest*, **39**, 2, 91-114
22. SERIANI G., 1994, 3-D large-scale wave propagation modeling by spectral element method on Cray T3E multiprocessor, *Computer Methods in Applied Mechanics and Engineering*, **164**, 1/2, 235-247
23. SERIANI G., PRIOLO E., 1994, Spectral element method for acoustic wave simulation in heterogeneous media, *Finite Elements in Analysis and Design*, **16**, 3/4, 337-348

24. SRIDHAR R., CHAKRABORTY A., GOPALAKRISHNAN S., 2006, Wave propagation in a anisotropic and inhomogeneous uncracked and cracked structures using pseudospectral finite element method, *International Journal of Solids and Structures*, **43**, 16, 4997-5031
25. STASZEWSKI W.J., MAHZAN S., TRAYNOR R., 2009, Health monitoring of aerospace composite structures – Active and passive approach, *Composites Science and Technology*, **69**, 11/12, 1678-1685
26. SU Z., YE L., 2009, *Identification of Damage Using Lamb Waves: From Fundamentals to Applications*, Berlin Heidelberg: Springer-Verlag
27. SU Z., YE L., LU Y., 2006, Guided Lamb waves for identification of damage in composite structures: A review, *Journal of Sound and Vibration*, **295**, 3/5, 753-780
28. WANG S., 2004, A finite element model for the static and dynamic analysis of a piezoelectric bimorph, *International Journal of Solids and Structures*, **41**, 15, 4075-4096
29. ZAK A., KRAWCZUK M., OSTACHOWICZA W., 2006, Propagation of in-plane waves in an isotropic panel with a crack, *Finite Elements in Analysis and Design*, **42**, 11, 929-941

Charakterystyki propagacji fal sprężystych w belkach grubych – w jakich przypadkach fala prowadzona jest falą dominującą?

Streszczenie

Praca przedstawia problem detekcji uszkodzeń w belkach o znacznej grubości za pomocą trójwymiarowej metody elementów spektralnych (SEM) ze szczególnym uwzględnieniem charakterystyk propagacji fal w ośrodku. Analiza rozchodzenia się fal w belkach o różnej grubości poddanych wymuszeniom o różnej częstotliwości centralnej ujawniła, że gdy grubość belki jest porównywalna z długością fali sprężystej, to oprócz quasi-symetrycznych i quasi-antysymetrycznych postaci pojawia się lokalna postać własna fali. Gdy długość fali przekracza co najmniej dwukrotnie grubość belki, postaci lokalne zanikają i postaci fal mogą zostać uznane jako tradycyjne fale prowadzone, tj. fale Lamba. Pokazano, że centralna częstotliwość sygnałów falowych może zostać dobrana do konkretnych rozmiarów belki tak, aby otrzymać proste postaci własne fal przypominające kształt fal rozchodzących się w belkach cienkich. W pracy zbadano charakterystyki propagacji fal w belce nieuszkodzonej i belce z pęknięciem poprzecznym. Rezultaty tych badań zweryfikowano doświadczalnie poprzez generowanie i rejestrację sygnałów w grubych stalowych belkach aktuatorami i czujnikami piezoelektrycznymi.

Manuscript received March 7, 2011; accepted for print March 17, 2011